

PRECISION MASSES OF THE LOW-MASS BINARY SYSTEM GJ 623

FRANTZ MARTINACHE¹, JAMES P. LLOYD¹, MICHAEL J. IRELAND², RYAN S. YAMADA¹, PETER G. TUTHILL³
Draft version October 11, 2018

ABSTRACT

We have used Aperture Masking Interferometry and Adaptive Optics (AO) at the Palomar 200" to obtain precise mass measurements of the binary M dwarf GJ 623. AO observations spread over 3 years combined with a decade of radial velocity measurements constrain all orbital parameters of the GJ 623 binary system accurately enough to critically challenge the models. The dynamical masses measured are $m_1 = 0.371 \pm 0.015 M_{\odot}$ (4%) and $m_2 = 0.115 \pm 0.0023 M_{\odot}$ (2%) for the primary and the secondary respectively. Models are not consistent with color and mass, requiring very low metallicities.

Subject headings: binary, stars: luminosity functions, mass functions, techniques: AO, interferometric

1. INTRODUCTION

The mass of a star, along with its metallicity and age, is the fundamental parameter that determines its position along an evolutionary track. Even if binarity, rotation, magnetic fields and other parameters also affect stellar interiors, what is known as the Vogt-Russel theorem remains an important rule, and the mass an essential parameter of stellar evolution. Binary systems offer the ideal test to infer dynamical masses independent of the use of a stellar model such as those of Baraffe et al. (1998), or an empirical mass-luminosity (hereafter M/L) relation. Such relations, available for both visible (Henry et al. 1999) and near infrared (Delfosse et al. 2000) are important astrophysical tools, fairly well constrained for intermediate mass stars. However, the Solar neighborhood is dominated by low mass stars, in both number and total mass (Henry 1998), and as dust condenses in the atmospheres of these cool stars, the models meet new unknowns. There also are puzzles in the stellar structure of M dwarfs and the extrapolation of these models to substellar objects remains untested. Below $0.6 M_{\odot}$, both M/L relations and models will benefit from model-independent determinations of high precision stellar masses, which can be achieved by combining radial velocimetry measurements and high angular resolution imaging (Delfosse et al. 2004; Ségransan et al. 2000). The complementarity of the two techniques yields substantial benefits, even in the regime where the time baseline of the observations is shorter than the orbital period (Eisner & Kulkarni 2002).

We have observed known M dwarfs binaries with precise radial velocity measurements published by Nidever et al. (2002). These late type M dwarfs are ideal observing targets for imaging with the PALAO Adaptive Optics (AO) system and the PHARO infrared camera (Hayward et al. 2001), optimized for the near infrared bands. At small angular separation (*i.e.* $< 2\lambda/d$), the sensitivity of the detection of faint companions can be improved by combining AO with aperture masking interferometry (Lloyd et al. 2006; Pravdo et al. 2006). This pa-

per provides the astrometry of the binary system GJ 623, successfully observed with both AO and AO + aperture masking. Combined with the radial velocity measurement, the astrometry provides precise dynamical masses (better than 2%) of the GJ 623 binary system. Combined with the J,H,K photometry, this measurement adds new constraints to the models and M/L relations.

2. THE OBSERVATIONS

2.1. *The primary*

GJ 623 (aka LHS 417, HIP 80346) is a high proper motion M2.5 dwarf 8 pc from the Sun. It is a long known astrometric binary, first characterized by Lippincott & Borgman (1978). GJ 623 has proven to be a ideal test for different observational techniques, such as radial velocimetry (Marcy & Moore 1989; Nidever et al. 2002) and speckle interferometry (McCarthy & Henry 1987). This binary system has also been directly imaged in the visible with the COSTAR corrected HST/FOC (Barbieri et al. 1996).

Our observations of GJ 623 were performed with the PHARO instrument on the Palomar 200" telescope and with the NIRC2 instrument on the Keck II telescope. The companion of GJ 623 was detected in six observing runs: September 2003, June 2004, January 2005 and February 2006, at Palomar, using J, H and K_s filters, and June and August 2006 at Keck, with the 1.58 μm H_{cont} filter. Tables 1 and 2 respectively gather the astrometric and photometric measurements made at Palomar and Keck.

Four of our observations consist of conventional direct imaging with AO. These images were dark subtracted, flat fielded and analysed with a custom IDL program, using the latest PHARO and NIRC2 plate scale and orientation characterization by Metchev & Hillenbrand (2004). The location of the companion (angular separation and position angle) and the contrast ratio are precisely determined with a cross correlation of the images. Not surprisingly, doubling the diameter of the telescope (*c.f.* the Keck data points) significantly improves the precision of the measurements and roughly reduces the error bars by a factor 3.

The data also include observations in aperture masking interferometry with AO. This technique (Tuthill et al. 2000), recently described by Lloyd et al. (2006), is appropriate to the detection of faint companion at small

¹ Department of Astronomy, Cornell University, Ithaca NY

² Division of Geological and Planetary Sciences, California Institute of Technology, Pasadena CA

³ School of Physics, University of Sydney, Sydney NSW Australia

angular separation (typically less than $2 \lambda/D$), where direct AO imaging has so far proven difficult.

Indeed, present AO systems focus on achieving high contrast at moderate angular separation $> 4\lambda/D$. Below this limit, the variance of the speckle background dominates the photon noise by several orders of magnitude (Racine *et al.* 1999). This prevents us from calibrating the Point Spread Function (PSF), with a precision sufficient to discriminate faint companions from the bright star's residual speckles.

This issue can be evaded by using interferometric techniques. By sampling a few spatial frequencies only, a mask located in the pupil plane permits us to completely decompose the PSF into a finite set of Fourier components. Non-redundancy of the baselines passed by the mask ensures that each frequency is sampled only once and the visibilities can be used to form closure phases (Baldwin *et al.* 1986; Nakajima *et al.* 1989; Readhead *et al.* 1988). This observable rejects both atmospheric noise and calibration errors of the wavefront sensor. The only drawback is the transmission of such a mask: between 5 and 15 % for the ones used at Palomar. However, in the speckle noise limited regime, light loss does not result in a loss of sensitivity.

Our analysis also uses a HST observation dating to 1994, and originally published by Barbieri *et al.* (1996): an angular distance of 330 ± 20 mas and a position angle of $7.0 \pm 2.6^\circ$ on June 11, 1994. Even though this is inferior to the precision achieved with Palomar and Keck, which are much larger telescopes, the fact that this observation was performed more than 10 years ago adds an important constraint on the period of the binary.

Julian Date (-2450000)	Band	Pupil (see text)	Sep. (mas)	PA (deg)
2896.6	K _s	9 hole	240.4 ± 9.7	79.31 ± 2.0
3163.8	[Fe II]	18 hole	340.5 ± 20.4	49.16 ± 4.3
3402.1	K _s	full ap.	350.7 ± 2.2	28.66 ± 0.5
3780.0	J,H,K _s	full ap.	257.1 ± 3.1	-12.76 ± 0.6
3909.5	H _{cont}	Nirc2	176.7 ± 1.1	318.2 ± 0.2
3962.3	H _{cont}	Nirc2	138.7 ± 0.9	295.4 ± 0.2

TABLE 1
ASTROMETRIC MEASUREMENTS AT PALOMAR AND KECK:
ANGULAR SEPARATION AND POSITION ANGLE OF GJ 623 B.

Julian Date (-2450000)	Filter	Δmag
2896.6	K _s	3.051 ± 0.826
3163.8	Fe II	2.903 ± 0.476
3402.1	K _s	2.604 ± 0.047
3780.0	J	2.691 ± 0.038
	H	2.860 ± 0.039
	K _s	2.789 ± 0.014
3909.5	H _{cont}	2.794 ± 0.033
3962.3	H _{cont}	2.781 ± 0.016

TABLE 2
PHOTOMETRIC MEASUREMENTS OF GJ 623 B.

From the 2MASS catalog, the apparent magnitudes of GJ 623 AB are $J = 6.638 \pm 0.024$, $H = 6.141 \pm 0.021$ and $K = 5.915 \pm 0.023$.

The Hipparcos parallax $\pi = 124.34 \pm 1.16$ mas originally published by Perryman *et al.* (1997) was based on the radial velocimetry measurement of Marcy & Moore (1989). The parallax was recalculated by Jancart *et al.* (2005) after the publication of an improved radial velocity curve by Nidever *et al.* (2002). It is this revised parallax $\pi = 125.81 \pm 1.19$ mas (Pourbaix, D., *priv. comm.*) that we adopt here. The following absolute magnitudes can be deduced for GJ 623 AB: $M_J = 7.137 \pm 0.052$, $M_H = 6.640 \pm 0.051$ and $M_K = 6.414 \pm 0.052$.

3. METHOD: EXTRACTING ORBITAL PARAMETERS

The starting point in the determination of the orbital parameters of the GJ 623 system, is the set of radial velocity measurements published by Nidever *et al.* (2002) and available in the online version of the *Ninth Catalogue of Spectroscopic Binary Orbits* (Pourbaix *et al.* 2004) at <http://sb9.astro.ulb.ac.be>. The parameters deduced from the Keplerian fit to the data are summarized in table 3. They have been directly used by Jancart *et al.* (2005) to reprocess the *Hipparcos Intermediate Astrometric Data* of van Leeuwen & Evans (1998) for a complete characterization of the dynamical elements of the system.

The approach detailed in this paper consists of combining together, with no a priori assumptions, the original radial velocity data and our astrometric observations.

3.1. Keplerian Orbits

One uses the standard 2-body solution to parametrize the location of the companion orbiting GJ 623 A. To an observing date t , one associates an angle M called the mean anomaly:

$$M(t) = \frac{2\pi}{P}(t - T_P), \quad (1)$$

where P and T_P respectively represent the orbital period and the epoch at the periastron passage. In the orbital plane, the (x, y) coordinates can simply be expressed as a function of another angle, the eccentric anomaly E . It is the angle between the direction of the periastron and the current position of the companion, projected onto the ellipse's circumscribing circle perpendicularly to the major-axis, measured at the center of the ellipse (*c.f.* fig. 1):

$$M(E) = E - e \sin E \quad (2)$$

$$x(E) = a(\cos E - e) \quad (3)$$

$$y(E) = a\sqrt{1 - e^2} \sin E, \quad (4)$$

where a and e respectively represent the semi-major axis and the eccentricity of the orbit. Eq. 2, is called Kepler's equation. One solves this equation *i.e.* finds the value of E associated with a given M by using the following classical iterative algorithm:

$$E_0 = M$$

$$E_{n+1} = M + e \sin E_n. \quad (5)$$

3.1.1. Radial Velocity Orbital Models

One can use the standard 2-bodies solution (eq. 3 and 4) to compute the coordinates of the primary component

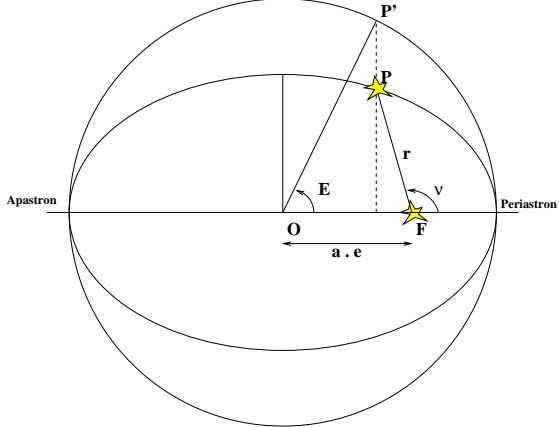


FIG. 1.— Parametrization of an elliptic orbit. Geometric relation between the excentric anomaly E and the true anomaly ν .

in the orbital plane, relative to the center of mass of the system:

$$\begin{bmatrix} x_P(E) \\ y_P(E) \end{bmatrix} = \frac{m_2}{m_T} \times \begin{bmatrix} x(E) \\ y(E) \end{bmatrix}, \quad (6)$$

where m_T and m_2 respectively stand for the total mass (primary + secondary) and the mass of the secondary. In the orbital plane, the velocity vector can be calculated with the following partial derivative:

$$V = \frac{\partial}{\partial t} \begin{bmatrix} x \\ y \end{bmatrix} = \frac{\partial}{\partial E} \begin{bmatrix} x \\ y \end{bmatrix} \times \frac{\partial E}{\partial M} \times \frac{\partial M}{\partial t}. \quad (7)$$

This derivation leads to the following x and y components of the velocity:

$$\begin{bmatrix} v_x(E) \\ v_y(E) \end{bmatrix} = \frac{m_2}{m_T} \times \frac{2\pi a}{P(1 - e \cos E)} \begin{bmatrix} -\sin E \\ \sqrt{1 - e^2} \cos E \end{bmatrix}. \quad (8)$$

The Radial Velocity (hereafter RV) is the component of this velocity projected on the line of sight. Its expression therefore involves both the argument of the periastron ω_0 and the inclination of the system i . The RV is not sensitive to the orientation of the system on the sky, *i.e.* to the value of the argument of the ascending node Ω_1 :

$$RV(E, \omega_0, i) = [v_x(E) \sin \omega_0 + v_y(E) \cos \omega_0] \sin i + V_0 \quad (9)$$

where V_0 is a constant term, the mean RV.

3.1.2. Astrometric Orbital Models

Unlike the case of RV data for which equations are expressed from the center of mass of the system, the astrometric measurements gathered in Table 1 provide the instant position of the companion relative to the primary. In this frame, the trajectory of the companion is an ellipse, whose focus is the primary component. The parametric equation of this ellipse is:

$$r(\nu) = \frac{a(1 - e^2)}{1 + e \cos \nu}, \quad (10)$$

where a is the semi-major axis, e , the eccentricity ($0 < e < 1$) and ν , an angle called the true anomaly, which

is the angle between the direction of the periastron and the current position of an object on its orbit (P on fig. 1), measured at the focus of the ellipse.

Fig. 1 illustrates the one-to-one correspondence between eccentric and true anomaly. The projection of the point P on the major axis provides the following relation:

$$r \cos \nu = a(\cos E - e). \quad (11)$$

Together, eq. 10 and 11 lead to the primary to secondary distance r and the true anomaly ν , as functions of the eccentric anomaly E :

$$r = a(1 - e \cos E), \quad (12)$$

$$\cos \nu = \frac{\cos E - e}{1 - e \cos E}. \quad (13)$$

At a given observing date t , one needs once more to solve Kepler's equation (*c.f.* eq. 2) to determine the corresponding eccentric anomaly E . The location of the companion along the orbit is provided by eq. 12 and 13.

Contrary to the radial velocity, which is the component of the velocity projected on the line of sight, one measures here the position of the companion projected on the celestial sphere. Right ascension α and declination δ of the secondary (relative to the primary) are given by the following relations:

$$\alpha = r \times [\cos(\nu + \omega_0) \sin \Omega_1 + \sin(\nu + \omega_0) \cos i \cos \Omega_1] \quad (14)$$

$$\delta = r \times [\cos(\nu + \omega_0) \cos \Omega_1 - \sin(\nu + \omega_0) \cos i \sin \Omega_1]. \quad (15)$$

3.2. χ^2 fitting

We use the model presented in the previous section, to fit a 9 parameter model to 26 observables. The observables are 2 coordinates for 7 astrometric data points and 12 radial velocities. The 9 parameters are the 6 orbital elements, *i.e.* the semi-major axis a , the eccentricity e , the longitude of the ascending node ω_0 , the inclination i , the argument of periastron Ω_1 and the orbital period P , plus the RV offset V_0 and the semi-amplitude of the RV curve K_1 .

In the case of a conventional analysis of RV data, the main observable is the semi-amplitude K_1 , which once combined with the period and the eccentricity of the orbit, provides the mass function:

$$f(M_1, M_2, i) = \frac{M_2^3 \sin i^3}{(M_T)^2}. \quad (16)$$

This combined analysis RV+astrometry allows us to separate the geometrical effects from the semi-amplitude. This produces another composite observable, somewhat simpler than K_1 , a “pseudo-amplitude”, whose formal expression is:

$$A_1 = \frac{M_2}{M_T} \times \frac{2\pi a}{P}. \quad (17)$$

This is the parameter that will be used to determine the dynamical masses of the two components of the binary. The final result of this 9 parameter fit, with 17 degrees of

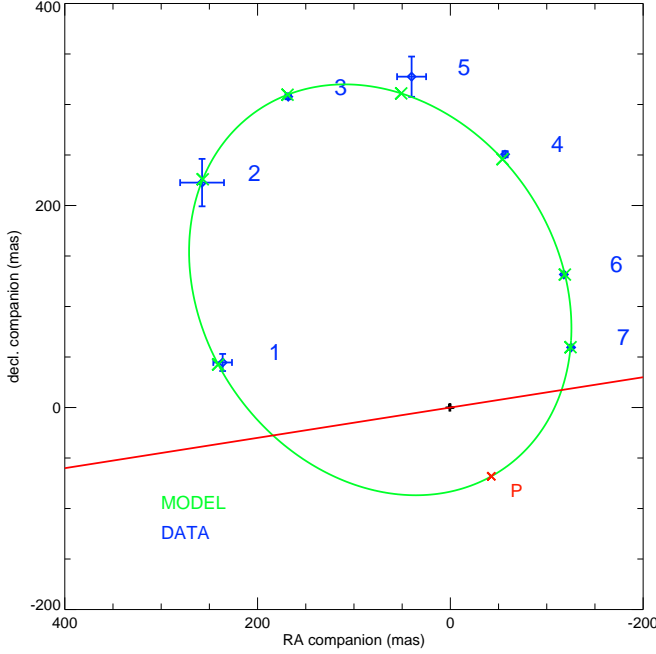


FIG. 2.— Orbit of GJ 623B. Measurements and associated uncertainties are represented in blue. Points 1-4: PHARO observations, point 5: Hubble observations reported in (Barbieri et al. 1996) and points 6-7: Nirc2 observations. In green, the Keplerian fit to the orbit. The red line is the line of nodes, the point P marks the position of the Periastron.

freedom is represented on Figure 2 for the astrometry and 3 for the radial velocimetry. Our solution exhibits a final reduced $\chi^2_\nu = 1.03$, which is, despite the heterogeneity of the data, close enough to unity to ensure confidence in our estimation of the error bars. It is dominated by the velocimetry, despite having fewer measurements than the astrometry.

The confidence interval of each of the parameters is determined by analysis of the likelihood function. If we assume that the noise associated to our measurements is Gaussian, and that our parameters are independent, the likelihood can be approximated by:

$$L(\text{parameters}) \propto \exp\left(-\frac{\chi^2}{2}\right). \quad (18)$$

The computation of a 9-dimensional likelihood function requires a lot of CPU time. This difficulty may be circumvented by confining the search to a subset of the total space. This is achieved by fixing the values of certain parameters and calculating the joined likelihood for the remaining parameters. However, one needs to check *a posteriori* that the validity of the hypothesis of independent parameters.

This analysis reveals that among the 9 parameters, only the argument of the periastron ω_0 and the longitude of the ascending node Ω_1 exhibit significant correlation. These two parameters are constrained within 0.5° (*c.f.* Table 3). The hypothesis of independent parameters is valid, as expected from our good coverage in both radial velocimetry and astrometry. The uncertainty associated to each parameter is taken equal to the standard deviation of its associated likelihood function.

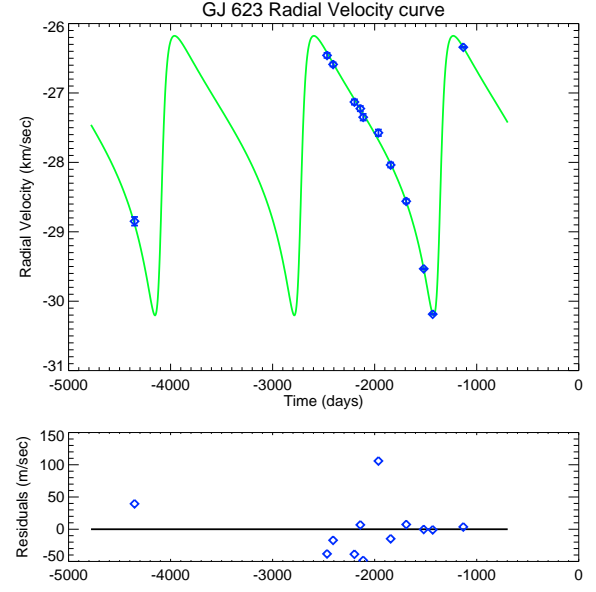


FIG. 3.— Radial Velocity curve of GJ 623A. The measurements and associated uncertainties reported by (Nidever et al. 2002) are represented in blue. The green solid line represents the Keplerian orbit with the parameters derived by χ^2 fitting.

The Gaussian-like likelihoods of the parameters used in the determination of the dynamical masses are shown on Fig. 4.

4. CHARACTERISTICS OF GJ 623 AB

The orbital parameters and the confidence intervals derived from the likelihood analysis are summarized in Table 3. This combined analysis significantly improved the constraints on the epoch at periastron passage, from $T_P = 2451298 \pm 10$ (Nidever et al. 2002) to the new value $T_P = 2451313.3 \pm 0.6$. The RMS of the Radial Velocity fit is 56 m/s for a semi-amplitude of $K_1 = 2.01 \pm 0.01$ km/s, which is comparable to the original fit (RMS=51 m/s for $K_1 = 2.08 \pm 0.04$ km/s).

parameter	Nidever	This work
Π (mas)	125.81 ± 1.19	
a (AU)	1.894 ± 0.019	
α (mas)	237.28 ± 0.88	
e	0.67 ± 0.01	0.631 ± 0.002
i (deg)		$154.0 \pm 0.1^\circ$
Ω_1		$98.5 \pm 0.47^\circ$
ω_0	$251 \pm 1^\circ$	$248.68 \pm 0.46^\circ$
P (days)	1366.1 ± 0.4	1365.6 ± 0.3
T_P (reduced JD)	1298 ± 10	1313.3 ± 0.6
V_0 (km/s)	-27.654 ± 0.3	-27.729 ± 0.005
A_1 (km/s)		3.57 ± 0.01

TABLE 3
ORBITAL ELEMENTS

4.1. Dynamical masses

From the data summarized in Table 3, one can determine the dynamical masses of both components of the

GJ 623 precision masses

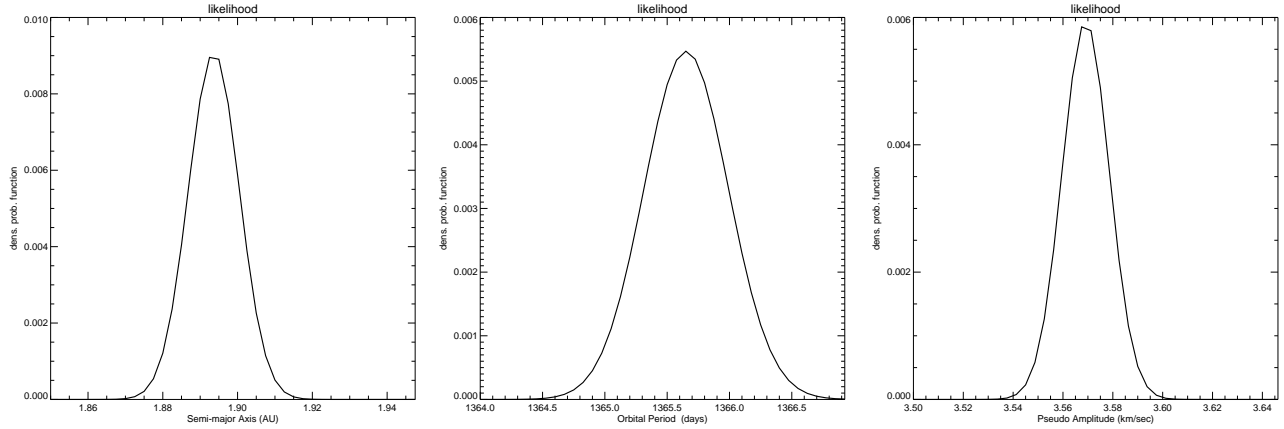


FIG. 4.— Likelihood functions of semi-major axis a , period P and radial velocity pseudo-amplitude A_1 , used to determine the dynamical masses of the GJ 623 system.

system. The revised parallax figuring in the table takes the binarity into account. The semi-major axis a , expressed in AU, once combined with the orbital period, gives the total mass M_T and the associated uncertainty σ_T :

$$M_T = a^3/P^2 \quad (19)$$

$$\sigma_T/M_T = \sqrt{(3\sigma_a/a)^2 + (2\sigma_P/P)^2}. \quad (20)$$

The likelihood analysis also determines the “pseudo-amplitude” defined by equation 17 and its associated uncertainty.

This composite parameter, combined with the total mass, allows independent determination of the mass of the secondary M_2 :

$$M_2 = M_T \times \frac{A_1 \times P}{2\pi a} = \frac{A_1 \times a^2}{2\pi P}, \quad (21)$$

$$\sigma_2/M_2 = \sqrt{(\sigma_{A_1}/A_1)^2 + (\sigma_P/P)^2 + (2\sigma_a/a)^2}, \quad (22)$$

and the mass ratio M_2/M_T :

$$M_R = \frac{m_2}{M_T} = \frac{A_1 \times P}{2\pi a}, \quad (23)$$

$$\sigma_R/M_R = \sqrt{(\sigma_{A_1}/A_1)^2 + (\sigma_P/P)^2 + (\sigma_a/a)^2}. \quad (24)$$

A similar analysis is possible for M_1 . Errors on the masses are dominated by the uncertainty on the semi-major axis, itself dominated by the error on the Hipparcos parallax. As a consequence, with a fractional error of 1 %, the mass ratio is better constrained than the mass of the secondary. The dynamical masses of the GJ 623 system are summarized in Table 4.

Quantity	Value
Total Mass	$M_T = 0.486 \pm 0.015 M_\odot$
Primary Mass	$M_1 = 0.371 \pm 0.015 M_\odot$
Secondary Mass	$M_2 = 0.115 \pm 0.0023 M_\odot$

TABLE 4
DYNAMICAL MASSES

4.2. Color, Metallicity & Kinematics

The multi-wavelength contrast ratios found in Table 2 may be used to decomposed the observed combined magnitude of the binary system into magnitudes for individual components. One determines the following absolute magnitudes: $M_J = 7.224 \pm 0.052$, $M_H = 6.719 \pm 0.051$ and $M_K = 6.495 \pm 0.052$ for GJ 623 A and $M_J = 9.915 \pm 0.065$, $M_H = 9.512 \pm 0.052$ and $M_K = 9.269 \pm 0.053$ for GJ 623 B.

With $J - K$ color indices of 0.729 ± 0.074 and 0.646 ± 0.084 respectively for the primary and the secondary, the GJ 623 AB system is bluer than the Delfosse et al. (2000) empirical M/L relation. Therefore, we suspect GJ 623 is of low metallicity. From the Hipparcos proper motion $(1145.38, -452.37)$ mas/yr (Perryman et al. 1997) and the RV offset $V_0 = -27.4$ km/s determined from our model fit, one can calculate the Galactic space velocity $(U, V, W) = (-33, 14, -41)$ km/s after correction for standard solar motion.⁴ This velocity is consistent with an old disk population, and therefore of subsolar metallicity (Chiba & Beers 2000), which is consistent with both components being bluer than the average field object.

Figure 5 compares the location of both components of the GJ 623 system in a mass-luminosity diagram to the low mass population II models of Montalbán et al. (2000) for different metallicities. The trend we observe with these models (*c.f.* Fig. 5) supports GJ 623 AB being of subsolar metallicity. The model that best matches our measurements for the primary is for $[M/H] = -1.0$. For the secondary, the best model predicts a slightly lower mass of $0.110 \pm 0.001 M_\odot$ for $[M/H] = -2.0$. This large discrepancy in metallicity is inconsistent with the assumption of a co-eval binary. The very low metallicity for the secondary would be consistent with GJ 623 B belonging to the galactic halo, which is unlikely according to the kinematics. Therefore, we conclude that the models do not adequately fit the data.

5. CONCLUSION

⁴ The sign convention is the one of the IDL astrolib gal_uvw procedure. Note that the literature is confusing on this matter. For instance, McCarthy & Henry (1987) provide numbers of comparable magnitude but with opposite sign for all (U, V, W) components.

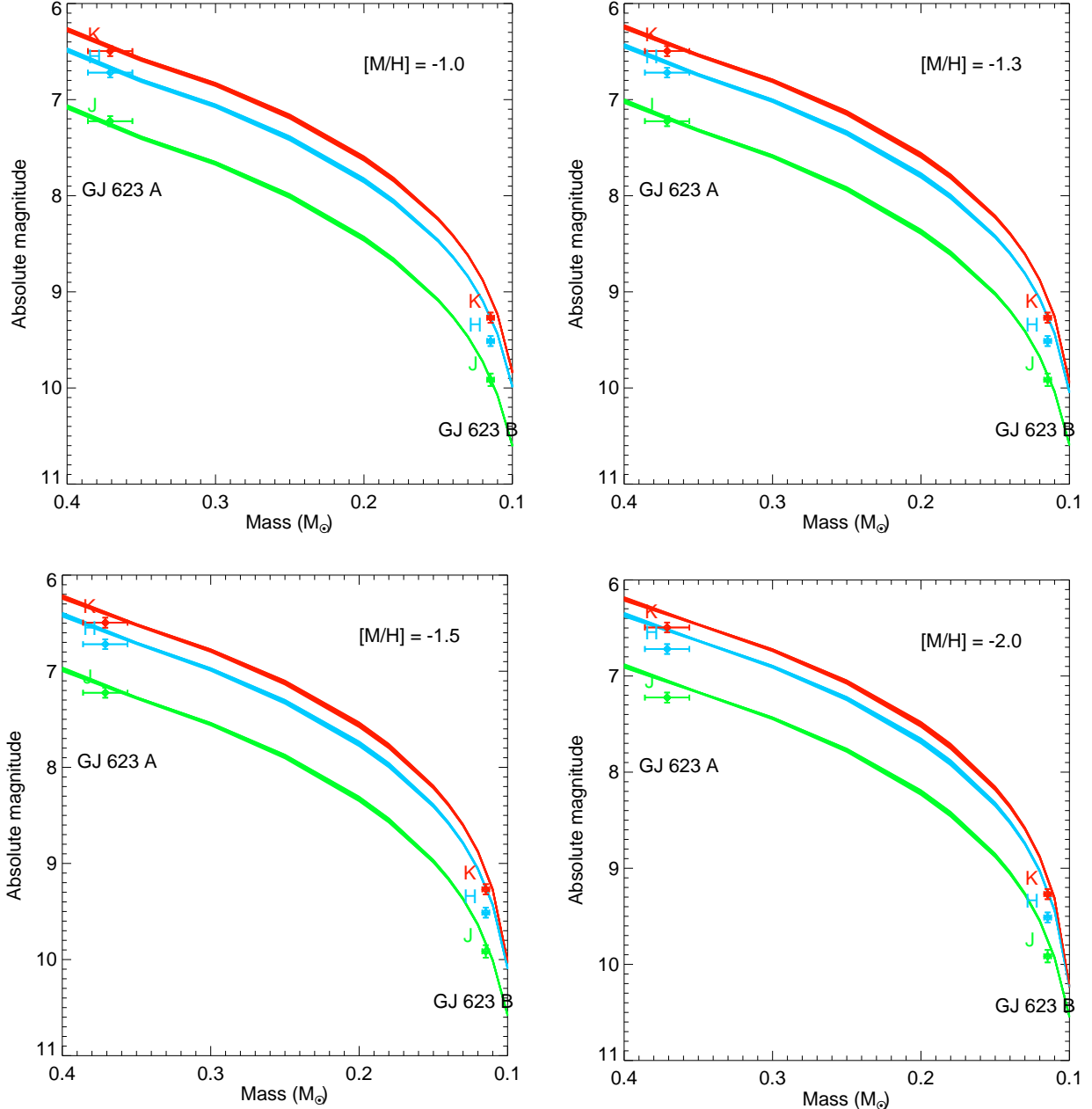


FIG. 5.— Mass-luminosity diagram for the GJ 623 system in J, H and K bands. Comparison with the low mass population II stars models by Montalbán *et al.* (2000) in the 0.1-0.4 solar mass range, for different metallicities.

The observation of binary systems is the only way to measure unbiased masses. As shown in this paper, combined with excellent radial velocity measurements, a few high angular resolution images provide sufficient information to constrain the range of possible masses below the 5% precision that is required to seriously challenge the models at the low end of the main sequence.

The application of precision RV methods developed for planet searches, combined with AO will provide a complete characterization of the stellar structure of the lower main sequence.

We thank the staff and telescope operators of Palomar

Observatory and Keck Observatory for their support. F.M. thanks Terry Herter for his help. This work is partially funded by the National Science Foundation under grants AST-0335695 and AST-0506588. This publication makes use of the Simbad database, operated at CDS, Strasbourg, France and the data products from the Two Micron All Sky Survey, which is a joint project of the University of Massachusetts and the Infrared Processing and Analysis Center/California Institute of Technology, funded by the National Aeronautics and Space Administration and the National Science Foundation. We wish to extend special thanks to those of Hawaiian ancestry on whose sacred mountain we are privileged to be guests.

Without their generous hospitality, the observations pre-

sented herein would not have been possible.

REFERENCES

Baldwin, J. E., Haniff, C. A., Mackay, C. D., & Warner, P. J. 1986, *Nature*, 320, 595

Baraffe, I., Chabrier, G., Allard, F., & Hauschildt, P. H. 1998, *A&A*, 337, 403

Barbieri, C., Demarchi, G., Nota, A., Corrain, G., Hack, W., Ragazzoni, R., & Macchett, D. 1996, *A&A*, 315, 418

Chiba, M. & Beers, T. C. 2000, *AJ*, 119, 2843

Delfosse, X., Beuzit, J.-L., Marchal, L., Bonfils, X., Perrier, C., Ségransan, D., Udry, S., Mayor, M., & Forveille, T. 2004, in *ASP Conf. Ser. 318: Spectroscopically and Spatially Resolving the Components of the Close Binary Stars*, ed. R. W. Hilditch, H. Hensberge, & K. Pavlovski, 166–174

Delfosse, X., Forveille, T., Ségransan, D., Beuzit, J.-L., Udry, S., Perrier, C., & Mayor, M. 2000, *A&A*, 364, 217

Eisner, J. A. & Kulkarni, S. R. 2002, *ApJ*, 574, 426

Hayward, T. L., Brandl, B., Pirger, B., Blacken, C., Gull, G. E., Schoenwald, J., & Houck, J. R. 2001, *PASP*, 113, 105

Henry, T. J. 1998, in *ASP Conf. Ser. 134: Brown Dwarfs and Extrasolar Planets*, ed. R. Rebolo, E. L. Martin, & M. R. Zapatero Osorio, 28–+

Henry, T. J., Franz, O. G., Wasserman, L. H., Benedict, G. F., Shelus, P. J., Ianna, P. A., Kirkpatrick, J. D., & McCarthy, Jr., D. W. 1999, *ApJ*, 512, 864

Jancart, S., Jorissen, A., Babusiaux, C., & Pourbaix, D. 2005, *A&A*, 442, 365

Lippincott, L. S. & Borgman, E. R. 1978, *PASP*, 90, 226

Lloyd, J. P., Martinache, F., Ireland, M. J., Monnier, J. D., Pravdo, S. H., Shaklan, S. B., & Tuthill, P. G. 2006, *ArXiv Astrophysics e-prints*

Marcy, G. W. & Moore, D. 1989, *ApJ*, 341, 961

McCarthy, Jr., D. W. & Henry, T. J. 1987, *ApJ*, 319, L93

Metchev, S. A. & Hillenbrand, L. A. 2004, *ApJ*, 617, 1330

Montalbán, J., D'Antona, F., & Mazzitelli, I. 2000, *A&A*, 360, 935

Nakajima, T., Kulkarni, S. R., Gorham, P. W., Ghez, A. M., Neugebauer, G., Oke, J. B., Prince, T. A., & Readhead, A. C. S. 1989, *AJ*, 97, 1510

Nidever, D. L., Marcy, G. W., Butler, R. P., Fischer, D. A., & Vogt, S. S. 2002, *ApJS*, 141, 503

Perryman, M. A. C., Lindegren, L., Kovalevsky, J., Hoeg, E., Bastian, U., Bernacca, P. L., Crézé, M., Donati, F., Grenon, M., van Leeuwen, F., van der Marel, H., Mignard, F., Murray, C. A., Le Poole, R. S., Schrijver, H., Turon, C., Arenou, F., Froeschlé, M., & Petersen, C. S. 1997, *A&A*, 323, L49

Pourbaix, D., Tokovinin, A. A., Batten, A. H., Fekel, F. C., Hartkopf, W. I., Levato, H., Morrell, N. I., Torres, G., & Udry, S. 2004, *A&A*, 424, 727

Pravdo, S. H., Shaklan, S. B., Wiktorowicz, S. J., Kulkarni, S., Lloyd, J. P., Martinache, F., Tuthill, P. G., & Ireland, M. J. 2006, *ApJ*, 649, 389

Racine, R., Walker, G. A. H., Nadeau, D., Doyon, R., & Marois, C. 1999, *PASP*, 111, 587

Readhead, A. C. S., Nakajima, T. S., Pearson, T. J., Neugebauer, G., Oke, J. B., & Sargent, W. L. W. 1988, *AJ*, 95, 1278

Ségransan, D., Delfosse, X., Forveille, T., Beuzit, J.-L., Udry, S., Perrier, C., & Mayor, M. 2000, *A&A*, 364, 665

Tuthill, P. G., Monnier, J. D., Danchi, W. C., Wishnow, E. H., & Haniff, C. A. 2000, *PASP*, 112, 555

van Leeuwen, F. & Evans, D. W. 1998, *A&AS*, 130, 157